Megahed *et al. J Wireless Com Network (2023) 2023:61*
https://doi.org/10.1186/s13638-023-02267-y

EURASIP Journal on Wireless Communications and Networking

RESEARCH **Open Access**

5G millimeter wave wideband MIMO antenna arrays with high isolation

Amany A. Megahed[1*], Ehab H. Abdelhay[2,3], Mohamed Abdelazim[2] and Heba Y. M. Soliman[4]

*Correspondence: engamany@yahoo.com

[1] Higher Institute of Engineering and Technology, New Damietta 41525, Egypt
[2] Electronic and Communication Department, Mansoura University, Mansoura 35516, Egypt
[3] Faculty of Engineering, Mansoura National University, Gamasa, Egypt
[4] Electronic and Communication Department, Port Said University, Port Fuad 42526, Egypt

Abstract

In this paper, a compact two-port MIMO antenna array system is described. The antenna array spans the range from 27 to 40 GHz, whereas the impedance of the antenna element is matched at 50 Ω. The gain of the antenna element is between 5.5 and 8.5 dBi, and its radiation efficiency is between 65 and 90%. With high impedance matching for 5G MMW (Millimeter Wave), particularly at 28 GHz and 38 GHz, the 2-port antenna array operates in the frequency range of 27–40 GHz. The suggested MIMO array operates effectively with a gain of approximately 10 dBi and a radiation efficiency of approximately 95%. The antenna array's overall dimensions are a length of 55.27 mm, a width of 27.635 mm, and a depth of 1.6 mm with partial ground. A FR-4 substrate is used in the antenna's fabrication, greatly reducing the cost. In the antenna array, a decoupling surface is used between the antennas, with orthogonality being maintained between the ports to reduce mutual coupling. The results of the modelling show a reduction in the measured mutual coupling between array ports of less than −35 dB. An envelope correlation coefficient (ECC) of less than 1×10^{-4} is preferable. Additionally, the channel loss capacity is less than 0.3 bits/s/Hz, the mean effective gain is approximately −6 dB, and the total active reflection coefficient is upgraded to be less than −30 dB. Moreover, a diversity gain of approximately 10 dB is achieved. The proposed construction was created using CST Microwave Studio 2019. When the antennas are constructed and tested, the experimental outcomes surpass those of the simulation. Each antenna element is 27.635 mm long, 27.635 mm wide, and 1.6 mm thick. Slots in the radiating circular patch antenna element could be used to improve the radiation characteristics across the intended bands. The parametric study specifies that the distance between the antenna elements should be 0.5 λ, where λ is the operational wavelength.

Keywords: 5G, MIMO, MMW, ECC, DG, MEG, TARC, CCL

1 Introduction

Several researchers have created antennas for 5G wireless systems as is shown in [1], where a tree patch antenna for 2.4 GHz ISM band applications with a gain of 7 dB is described. To support WLAN applications, [2] created a circular patch-type microstrip antenna. The antenna in [2] operates at 5.5 GHz with an efficiency of 79% and a gain of 3.2 dB. Additionally, many scholars presented various antenna shapes, such as those in [3–5]. The behaviour of fractal antennas and other non-Euclidean wire antennas in the range of low frequencies is covered in [3]. As in [6], in which the behaviours of of Sierpin-ski fractal antennas are discussed, [6–8] also addresses the behaviours of fractal antennas that operate on many bands. A discussion of a micro-strip fractal antenna with good directivity and broadband is provided in [8]. Multiple-input-multiple-output (MIMO) antenna technology is one of the most important components of 5G wireless communication networks. This approach enhances spectrum efficiency, cost efficiency, and energy efficiency. MIMO is frequently used in a variety of systems to significantly enhance channel capacities. Compact array antennas are widely used because of space limitations and aesthetic factors. A MIMO array with a gain of 2.5 dBi and a bandwidth ranging from 3.2 to 4 GHz is presented in [9]. Without any decoupling surfaces, [10] presented a 22 U-slot patch array antenna with a 13.1 dBi gain and a range spanning from 26.94 to 31.08 GHz.

Since the value of isolation is less than 14 dB, [11] employed the approach of DGS to obtain strong isolation between the input ports in a MIMO antenna array. The antenna is $45 \times 45 \times 1.6$ mm^3. The FR-4 substrate is used for the antenna's design. The range of frequencies is 2.2 GHz to 6.3 GHz. The design has a peak efficiency of approximately 91% and gain of approximately 4 dBi. To solve the mutual coupling issue, [12] used metamaterial loading techniques as well as DGS in the array design. An eight-port UWB MIMO antenna was developed in [13], and they used a parasitic decoupling structure to reduce mutual coupling.

A four-port MIMO array is created in [14]. The antenna has the following dimensions: a length of 30 mm, a width of 35 mm, and a depth of 0.76 mm. It operates in the frequency range of 25.5–29.6 GHz and has an antenna gain of 8.3 dBi. Nevertheless, [15] presented an 8-port MIMO array to cover the spectrum from 27.5 to 29.5 GHz with a Rogers Duroid 5880 substrate. Metamaterials are employed in [16–19] to provide excellent port isolation. Four-port MIMO arrays are introduced in [20] to support 5G, although its antenna array gain is just 5 dBi. With a bandwidth ranging from 26 GHz to more than 39 GHz, MIMO antenna arrays with high bandwidth and good characteristics are proposed in [21, 22]. In [23], the antenna achieves a 20 dBi gain with an overall gain of 8 dBi and covers a band between 24 GHz and 40 GHz. In this research, an orthogonal two-port MIMO antenna array is proposed to reduce mutual interaction. The proposed antenna array supports 5G MMW applications, namely, at 28 and 38 GHz. Moreover, the antenna can operate in the frequency range between 27 and 40 GHz. It is built on an FR-4 substrate, which has a dielectric constant of 4.3, to lower the cost of the antenna and simplify the structure. Each antenna element has a 50-ohm impedance match. Its antenna element gain is 10 dBi, and its radiation efficiency is 95%. The MIMO antenna is 55.27 mm in length, 27.635 mm in width, and 1.6 mm in thickness overall.

The following sections make up the remaining portions of the paper. The technique is employed in Sect. 2. In Section 3, details regarding the antenna element's design and configuration are provided. In Sect. 4, the two-port MIMO array design is explained. In Sect. 5, the MIMO results are presented and discussed. The results of the MIMO array parameters are provided in Sect. 6. The final section contains the conclusion.

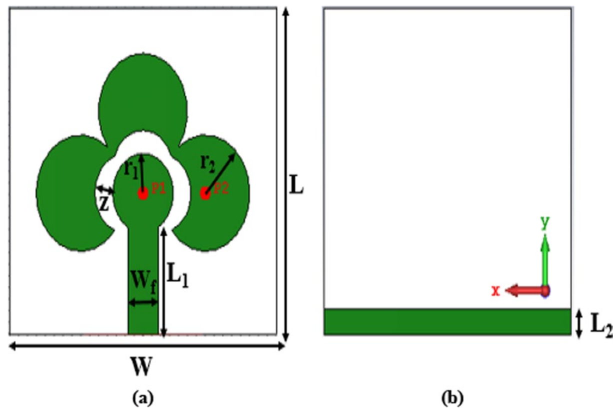

Fig. 1 Geometry of the array patch antenna element with an impedance of 50 Ω. **a** Front side. **b** Back side

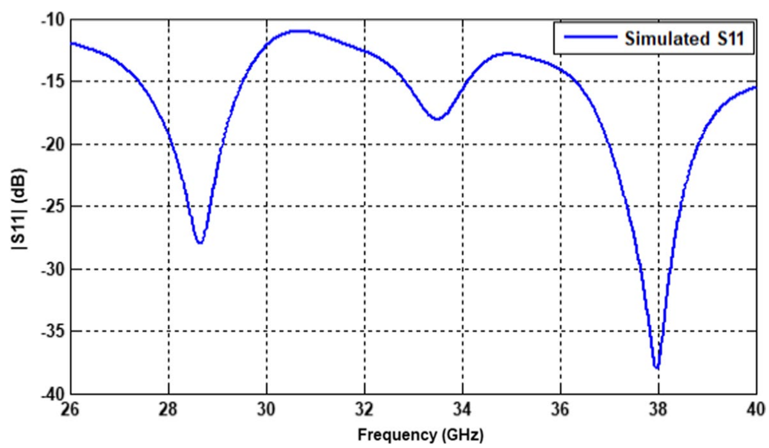

Fig. 2 Reflection coefficient of a single element

2 Method and experiment

The MIMO antenna array and antenna element are simulated using the CST program. To provide strong isolation between the antenna ports, a decoupling surface between the antennas is added into the ground plane.

3 Antenna element design

The concept behind the proposed antenna is to use a patch antenna's radiating element that has slots. The antenna is printed on an FR-4 substrate with a loss tangent value of 0.025 and a dielectric constant of 4.3. (Fig. 1). The patch's operating frequencies are 28 GHz and 38 GHz. The designed antenna covers the 5G MMW band (Fig. 2).

The patch antenna's bandwidth is determined by the circle's radius. The radius of the patch-circle antenna is determined using Eqs. (1) and (2) [1], where h is the substrate's height; εr and fr are the dielectric constant of the substrate and resonant frequency, respectively; and C is the speed of light, which equals 3×10^8 m/s. A portion of the antenna is grounded. The antenna element covers the range from 27 to 40 GHz with a 50-ohm impedance matching. The radiation efficiency and gain of each antenna element are 90% and 8.5 dBi, respectively.

$$r = \frac{F}{\left[1 + \frac{2h}{\pi F \epsilon_r}\left(\ln\left\{\frac{\pi F}{2h}\right\} + 1.7726\right)\right]^{0.5}} \tag{1}$$

$$F = \frac{8.791*10^9}{f_r} \tag{2}$$

Table 1 provides the optimized values of the antenna parameters. According to Figs. 3 and 4, the antenna's efficiency and gain are set to 90% and 8.5 dBi, respectively. Figure 5 depicts the simulated two-dimensional (2D) beam forming at 28 GHz and 38 GHz with Φ= 90° and Θ= 90°. Notably, the E-plane antenna radiation pattern is omnidirectional. The corresponding vector current distribution for the recommended antenna element is shown in Fig. 6. Many different currents travel in different directions. The bandwidth will therefore increase by combining these currents. The patch antenna's feed line and

Table 1 Suggested antenna element optimized dimensions (in Millimeters)

W_f	3.3719	L_1	9.7	r_1	3.4	W	27.635
L	27.635	r_2	5	z	2	L_2	3

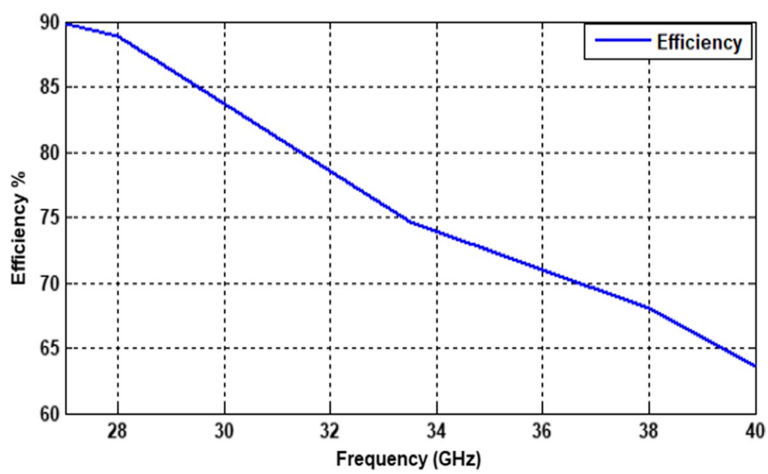

Fig. 3 Realized efficiency of the antenna versus the frequency

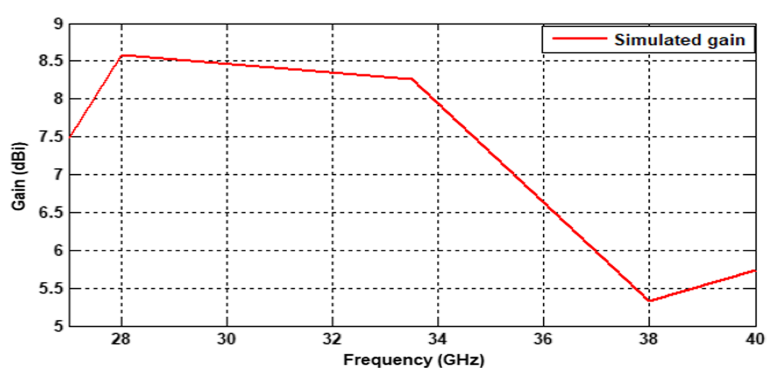

Fig. 4 Realized gain of the antenna

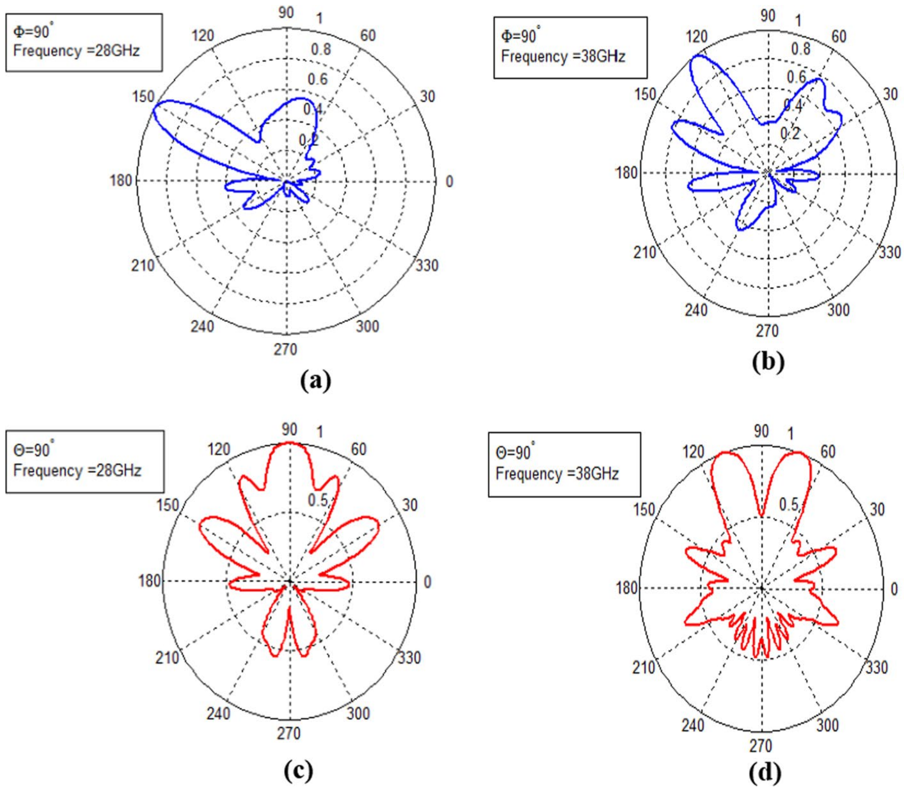

Fig. 5 Simulated beam-forming of a single element at $\Phi = 90°$ for the frequency of **a** 28 GHz, **b** 38 GHz and at $\Theta = 90°$ for the frequency of **c** 28 GHz, **d** 38 GHz

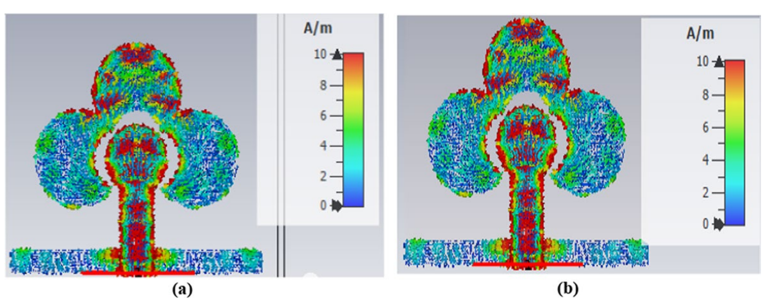

Fig. 6 Vector current density of the used antenna at **a** 28 GHz **b** 38 GHz

edges are where the flowing current is concentrated most heavily. Figure 7 illustration of the impedance, which is 50 ohms, indicates that good matching occurs. Table 2 lists the outcomes of the antenna element beam shaping.

4 Two-port MIMO antenna array design

The antenna element is simulated with the best dimensions in this research. The constructed antenna is made of an FR-4 substrate, which has a loss tangent of 0.025 and a dielectric constant of 4.3. The suggested MIMO array's optimum dimensions are Wx = 55.27 mm in length, Wy = 27.635 mm in width, and 1.6 mm in depth. The patch antenna's designed operating frequencies are 28 GHz and 38 GHz. The antenna element

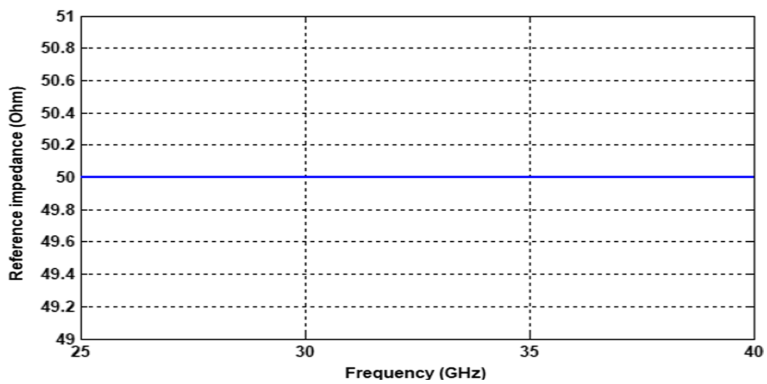

Fig. 7 Simulated reference impedance versus the frequency of the antenna operation

Table 2 Results of the antenna's radiation pattern

Freq (GHz)	Parameters at Θ = 90° plane			Parameters at Φ = 90° plane		
	HPBW	MLM	SLL	HPBW	MLM	SLL
28	32.4°	4.53 dBi	− 1.5 dB	25.7°	10.4 dBi	− 5.3 dB
33	30.2°	5.98 dBi	− 3.2 dB	18.3°	8.62 dBi	− 2.6 dB
38	25.7°	4.9 dBi	− 3.4 dB	21.6°	8.11 dBi	− 1.7 dB

HPBW: Half Power Beam Width, MLM: Main Lobe Magnitude, SLL: Side Lobe Level

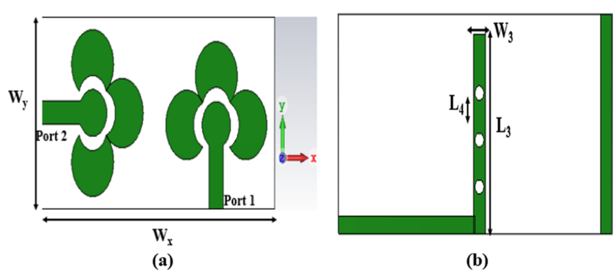

Fig. 8 Geometry of a 2-port MIMO. **a** Front side. **b** Backside

spacing is set to 0.5 λ, where λ is the operating wavelength. Using the commercial CST 2019 simulation tool, the planned MIMO antenna is tested (Fig. 8). The manufactured antenna is depicted in Fig. 9.

5 Results and discussion

Figure 10 presents the antenna's band-width, which ranges from 27 to 40 GHz at each port servicing the 5G MMW, together with the reflection coefficient at Ports 1 and 2. As shown in Fig. 8, the antenna elements are orthogonal to one another. To further reduce the mutual coupling between the ports because it serves as an isolating element between input ports, a decoupling surface with the dimensions L3 = 25 mm, W3 = 2.4 mm, and L4 = 5 mm is inserted between them in the ground plane. This structure also contains three slots in the shape of circles with a radius of 0.9 mm. As shown in Fig. 11, mutual coupling between the array ports is minimized by less than − 35

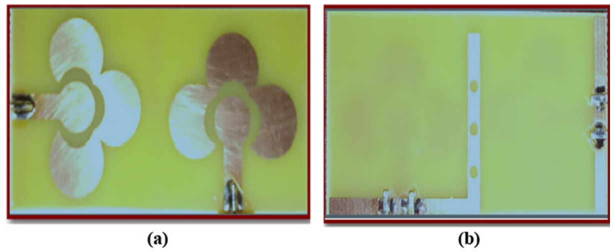

Fig. 9 Fabricated prototype of the proposed MIMO antenna. **a** Front side. **b** Back side

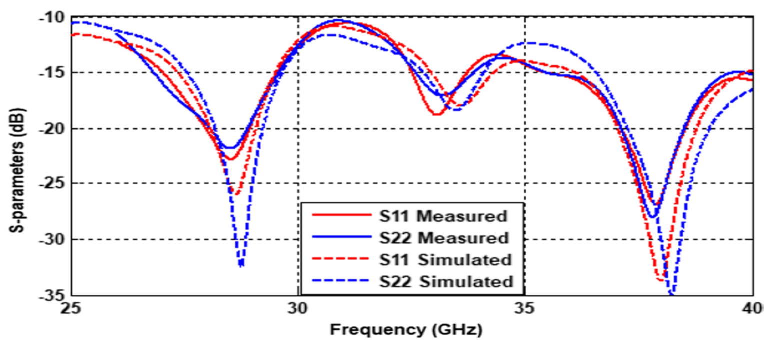

Fig. 10 Simulated and measured reflection coefficients at Ports (1) and (2)

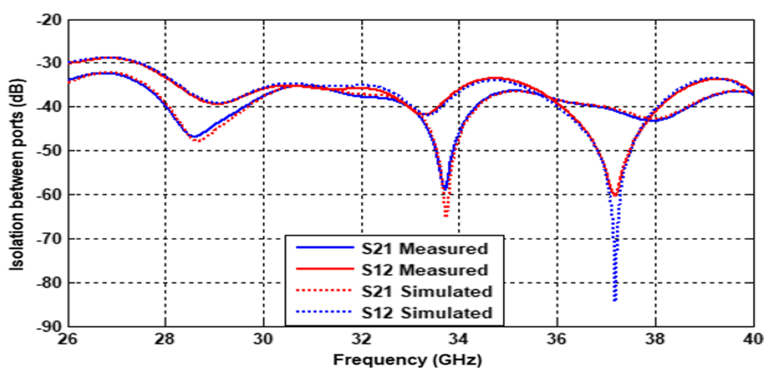

Fig. 11 Isolation coefficient between the ports

dB. The ground plane's isolating element and the additional capacitance added by the two antennas, as seen in Figs. 8 and 21, as well as the capacitance obtained through the dielectric gap between the top metallic patch and ground plane, are what reduce mutual coupling. Equations (3) and (4) are used to calculate the capacitance and inductance of the antenna elements, respectively [24]. The attained efficiency and gain are set to 95% and 10 dBi, respectively (Figs. 12 and 13). Fig. 14 displays the surface current at 28 GHz and 38 GHz while Port 1 is active. Although the isolation between the ports is less than − 15 dB, Fig. 15 shows the isolation between the ports without an isolation surface. The soldering of the SMA connector may account for the tiny discrepancy between the experimental and simulated results.

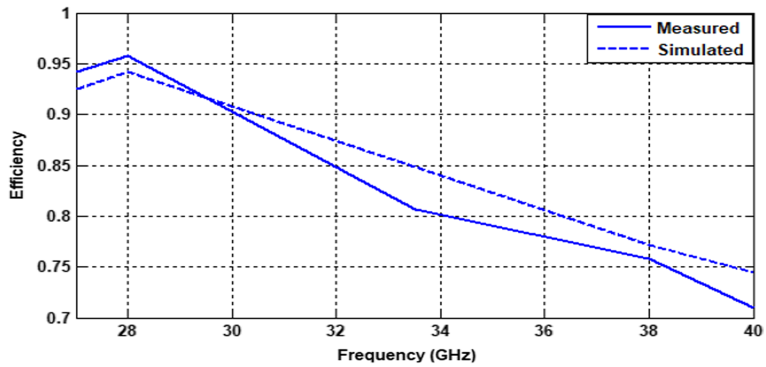

Fig. 12 Efficiency of the simulated and measured MIMO arrays

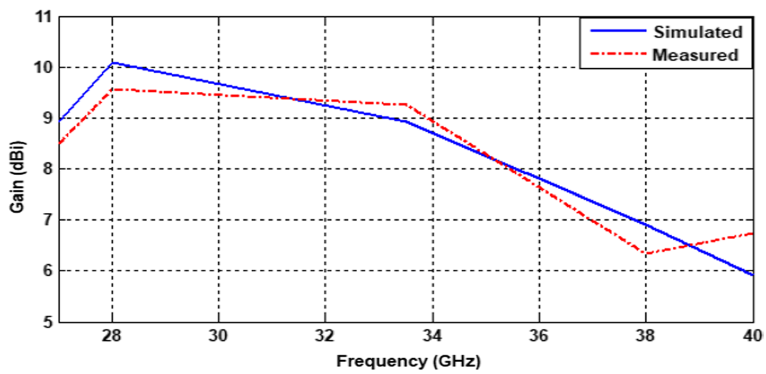

Fig. 13 Simulated and measured gain for the MIMO antenna

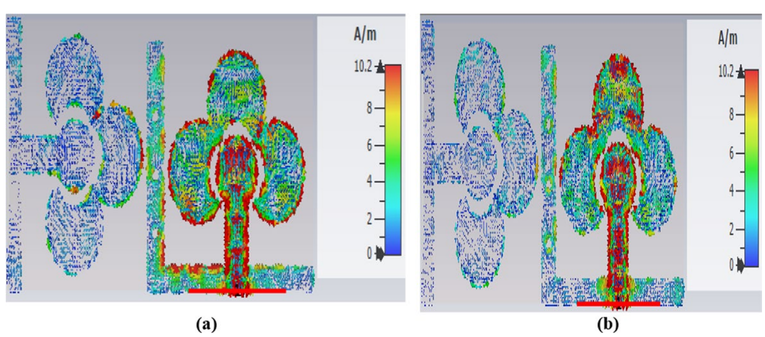

Fig. 14 Surface current at **a** 28 GHz, **b** 38 GHz when Port 1 is on

$$\mathrm{C_p} = \frac{2\mathrm{W_f}\varepsilon \mathrm{r}}{\mathrm{Lh}\omega_o^2} \tag{3}$$

$$\mathrm{L_p} = \frac{1}{\mathrm{C1}\omega_o^2} \tag{4}$$

where L is the total length of the patch and ω_o is the angular center frequency.

The E-plane beam-forming at frequencies of 28 GHz and 38 GHz is illustrated in Figure 16. The main lobe is focused at $\Phi = 90^\circ$ when $\theta = 90^\circ$, and they are orthogonal

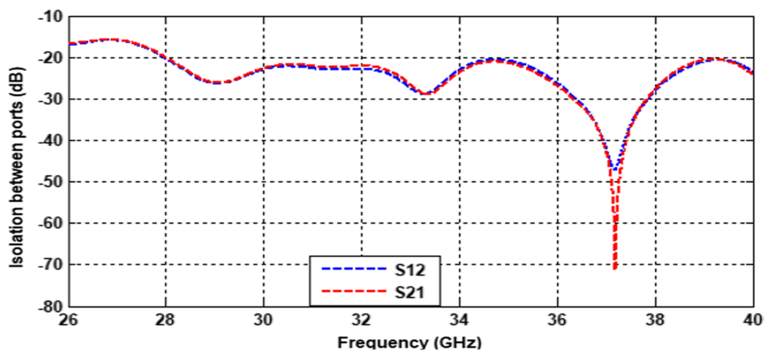

Fig. 15 Simulated isolation between the ports without the decoupling surface

because the two antennas are orthogonal, as shown in Figs. 16e–h. The beam form at θ = 90° with a frequency of 28 GHz for Port 1 is perpendicular to the radiation form at θ = 90° with a frequency of 28 GHz for Port 2, as shown in Figs. 16e and g. The beam-forming at θ = 90° with a frequency of 38 GHz for Port 1 is perpendicular to the radiation pattern at θ = 90° with a frequency of 38 GHz for Port 2, as shown in Figs. (f) and (h). Regarding the E-plane patterns when Φ = 0°, the maximum electric field is concentrated at θ = 30°, 60°, 150°, 210° and 330°, as drawn in Figs. (a), (b), (c) and (d). Moreover, with a low side lobe level, the E-plane patterns are identical across antennas, whereas at Φ = 90°, 60°, 150°, 210° and 330°, the patterns are more directive, as shown in Figs. (a), (b), (c) and (d). The beam-form was measured using a compact multiprobe antenna test station (STARLAB-18), which is a VNA type, in the antenna and microwave lab at the faculty of engineering at Ain Shams University in Egypt. The results of the MIMO array beam-forming at frequencies of 28 GHz, 33 GHz, and 38 GHz are shown in Table 3.

6 MIMO array parameters results

A variety of parameters are used to examine the MIMO array's quality. To analyze the MIMO antenna performance, one of the most crucial dynamic features for computing various parameters is used. The DG is expressed as the loss in the transmission power caused by the diversity schemes in a MIMO system. As shown in Fig. 17, the DG is approximately 10 decibels. The DG is determined through the next equation [18].

$$\mathrm{DG} = 10 \times \sqrt{1 - (\mathrm{ECC})^2} \tag{5}$$

One of the most important dynamic parameters for assessing the effectiveness of MIMO antennas is the ECC. The S-parameters can be used to compute this parameter as shown in the ensuing equation [14].

$$ECC = |S_{mm} \times S_{mn} + S_{nm} \times S_{nn}|^2 / \left(1 - |S_{mm}|^2 - |S_{nm}|^2\right) \times \left(1 - |S_{nn}|^2 - |S_{mn}|^2\right) \tag{6}$$

According to Fig. 18, the ECC result is 0.002.

The factor that certifies port coupling is the TARC. It is used to verify the effectiveness of a MIMO antenna. The TARC, which measures the total incident power, expresses the

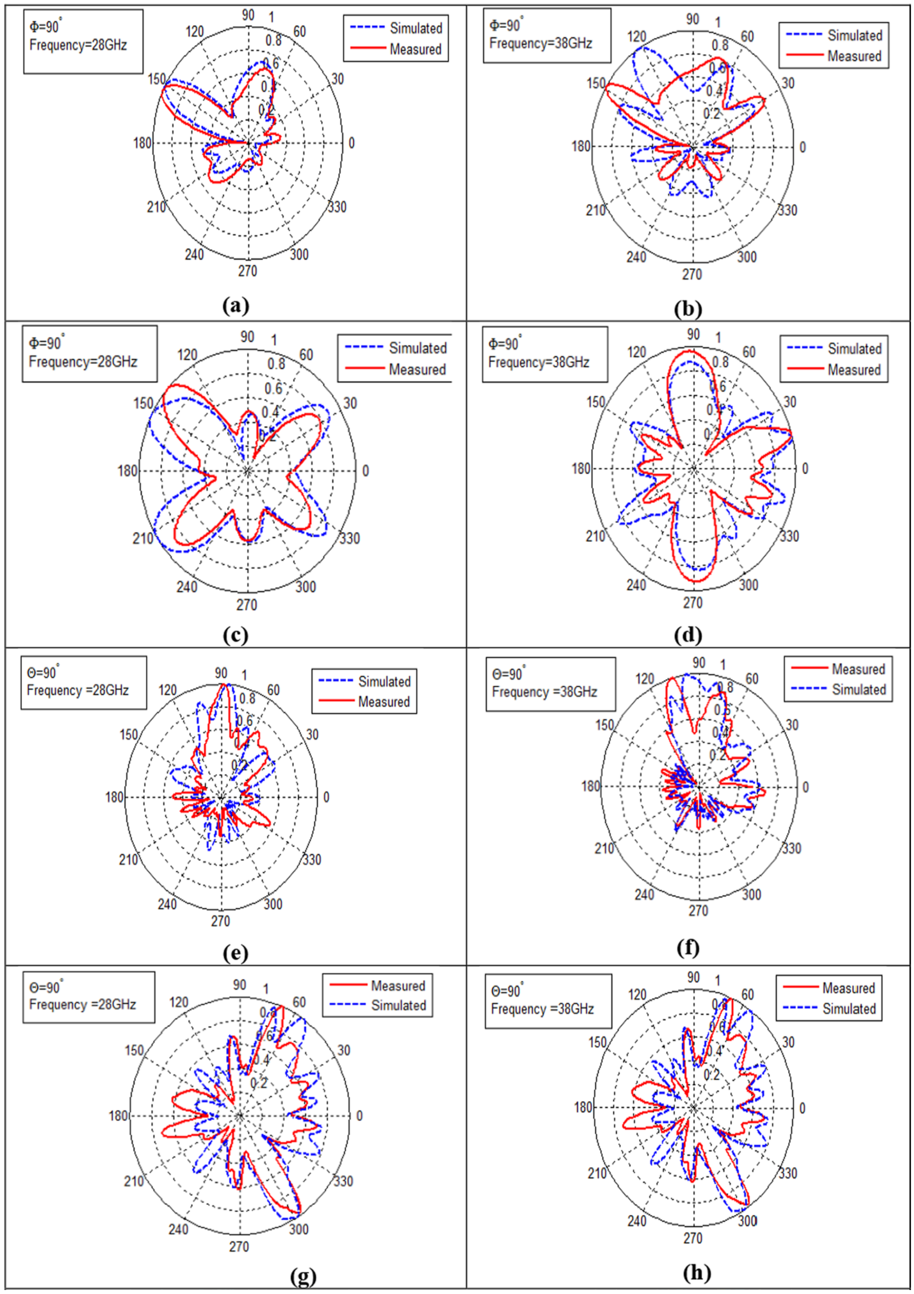

Fig. 16 Radiation pattern measured and simulated at Φ = 90° for Port 1 with **a** a frequency of 28 GHz, **b** a frequency of 38 GHz for Port 2, **c** a frequency of 28 GHz, **d** a frequency of 38 GHz at θ = 90° for Port 1, **e** a frequency of 28 GHz, **f** a frequency of 38 GHz for Port 2, **g** a frequency of 28 GHz, and **h** a frequency of 38 GHz

Table 3 Radiation pattern results of the MIMO array

Freq (GHz)	Θ = 90° plane			Φ = 90° plane		
	HPBW	MLM	SLL	HPBW	MLM	SLL
28	49.5°	4.87 dBi	− 1 dB	22.2°	7.9 dBi	− 2.2 dB
33	27.6°	6.42 dBi	− 3.3 dB	19.1°	10.7 dBi	− 4.3 dB
38	24.2°	5.1 dBi	− 1 dB	24.6°	8.61 dBi	− 3 dB

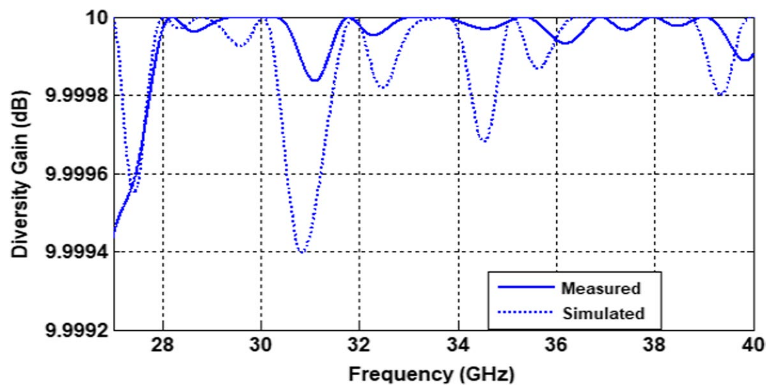

Fig. 17 DG for the two-port MIMO array

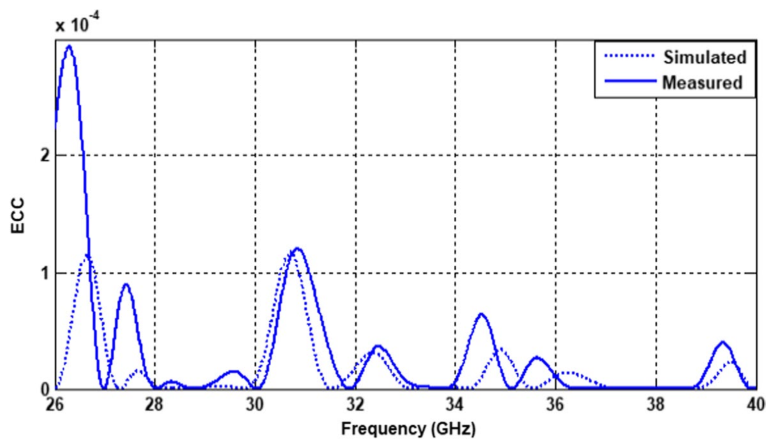

Fig. 18 ECC for the MIMO antenna over frequency

radiated power of the MIMO antenna array. The following equation [20] is used to calculate the TARC.

$$\Gamma = \frac{\sqrt{\left(\left|S_{mm} + S_{mn}e^{j\theta}\right|^2\right) + \left(\left|S_{nm} + S_{nn}e^{j\theta}\right|^2\right)}}{\sqrt{2}} \tag{7}$$

S_{mm} and S_{nn} are the corresponding reflection coefficients for Port 1 and Port 2, respectively, and $0° \leq \theta \leq 180°$ (θ: the angle of input phase) with a 30-degree step. Figure 19 depicts the TARC.

Several MIMO performance variables are considered to be major indicators of the channel capacity loss (CCL). The CCL is calculated using the following equation.

$$C\ loss = -\log_2\left(\Psi^R\right) \tag{8}$$

where ΨR is the receiving antenna correlation matrix, which is written as

$$\Psi R = \begin{matrix} \Psi_{mm} & \Psi_{mn} \\ \Psi_{nm} & \Psi_{nn} \end{matrix}$$

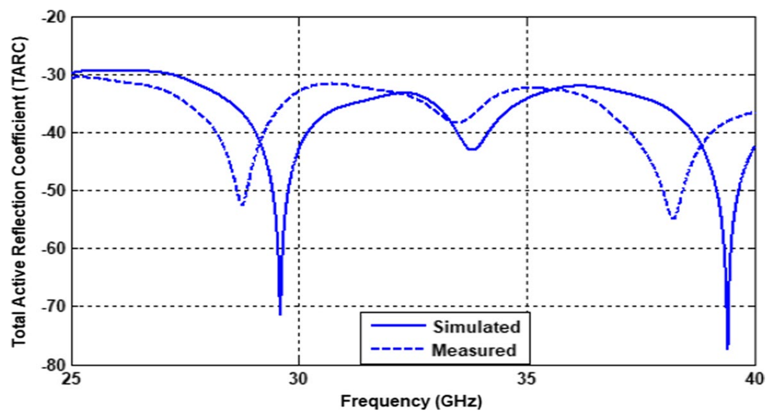

Fig. 19 TARC for the MIMO antenna over frequency

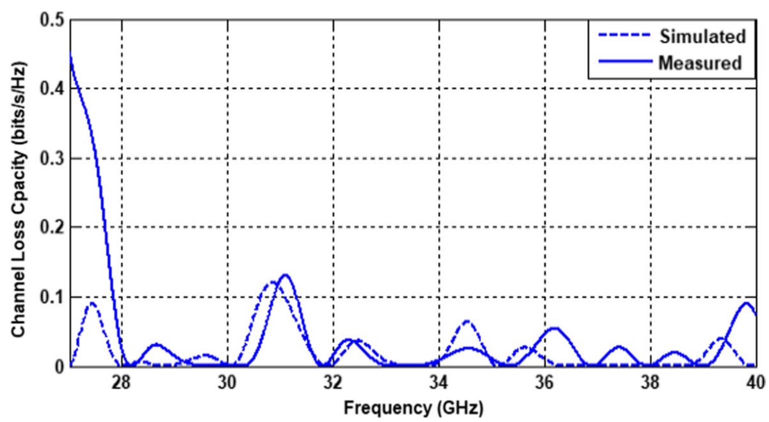

Fig. 20 CLL for MIMO antenna

where $\Psi_{mm} = 1 - (|S_{mm}|^2 + |S_{mn}|^2)$

$$\Psi_{mn} = -(S_{mm} * S_{mn} + S_{nm} * S_{nn})$$

$$\Psi_{nm} = -(S_{nm} * S_{nm} + S_{nm} * S_{nm})$$

$$\Psi_{nm} = 1 - (|S_{nm}|^2 + |S_{nm}|^2)$$

In the proposed designs, the CCL value is set to be less than 0.4 bits/sec/Hz; thus, it satisfies the requirements. Fig. 20 shows the resulting CCL.

The mean effective gain (MEG) provides the overall effectiveness, gain, and measurement of the antenna-channel mismatch. The MEG1/MEG2 ratios of the two antennas range from 0.9661 to 1.0076. Each antenna has an MEG value that ranges from 6.0146 dB to 6.5219 dB, as indicated in Table 4. The formulae below are used to calculate the MEG.

$$MEG_1 = 0.5 \times (1 - |S_{mm}|^2 - |S_{mn}|^2 \quad (9)$$

Table 4 Results of the MEG

FREQ (GHz)	(MEG)		
	MEG_1	MEG_2	MEG_1/MEG_2
28	− 6.3145	− 6.0146	0.9661
33	− 6.5219	− 6.4577	0.9926
38	− 6.3446	− 6.4107	1.0076

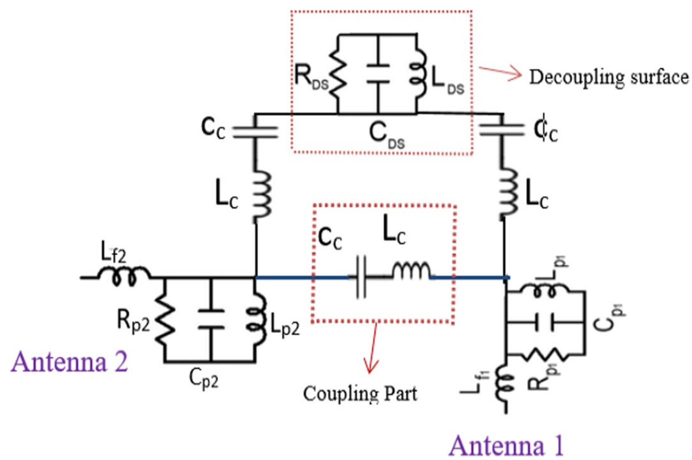

Fig. 21 Equivalent circuit of two port array with decoupling surface

$$MEG_2 = 0.5 \times (1 - |S_{mm}|^2 - \left||S_{mn}|^2\right|$$

In Fig. 21, which represents the equivalent circuit of a MIMO array with a decoupling surface. Moreover, the patch antenna is expressed as the resistance (Rp), inductance (Lp), and capacitance (Ca) (cp). In Table 5, the suggested antenna is contrasted with antennas that have been previously described in the literature.

7 Conclusion

Since the isolation is less than -35 dB, high isolation between the ports of a two-port MIMO array is introduced in this paper. Two circular patch array elements are made up of two antennas each with a circle-shaped slot to boost the bandwidth. An antenna is attached to a partially grounded aircraft. The antenna operates in the range from 27 GHz to 40 GHz to support the 5G MMW. The findings of the simulation and measurement have excellent agreement. The antenna arrays are built from a low-cost material with a substantial cost decrease. At less than 30 dB, it shows a good TARC performance. Moreover, the MEG is less than -6 dB, the ECC is less than 110-4, the DG approaches 10 dB, and the CCL is less than 0.3 bits/s/Hz. The antenna array is 55.27 x 27.635 mm2 in total size. The antenna array has a 10 dBi gain and a 95% efficiency.

Table 5 Performance evaluation of the proposed design against those of the previous literature

References	Number of ports	Type of substrate	Decoupling-method	Isolation improvement (dB)	Design -complexity	BW GHz	Size mm^3	DG	ECC	Gain (dBi)	Efficiency %
[9]	8	FR4	DGS	− 12	Easy	3.2:4	150 × 75 × 1.6	Not found	< 0.01	2.5	70
[10]	4	Rogers RT/ Duroid5880	–	− 12	Easy	28	41.3 × 46 × 0.508	Not found	Not found	13.1	Not found
[11]		FR4	Decoupling structure	− 14	Medium	5.2:5.8	42 × 42 × 0.8	Not found	Not found	5	80
[12]	6	FR4	Metamaterial pho-tonic bandgap	− 12	Easy	9.25:11	120 × 40 × 1.6	Not found	Not found	7.38	88%
[13]	4	FR4	Meta-surface	− 10	Easy	8.4:12.6 13.4:14.2 16.5:16.8 8.5:20.3	40 × 40 × 1.6	Not found	< 0.15	Not found	Not found
[14]	4	Rogers R04350B	DGS	− 20	Medium	25.5:29.6	30 × 35 × 0.76	> 9.96	< 0.01	8.3	82
[15]	8	Rogers Duroid 5880	–	− 20	Medium	27.5: 29.5	92.73 × 28.62 × 1.64	Not found	Not found	9.3	Not found
[16]	4	FR4	Metamaterial	− 15	Easy	9.12:9.96	40 × 40 × 1.6	Not found	Not found	5.4	Not found
[17]	2	FR4	Fractal load	− 13	Easy	8.7:17.1 22:26 29:34.2	70 × 37 × 1.6	Not found	Not found	9	93%
[18]	2	FR4	MTM-DS	− 15	Easy	9.95:10.63	40 × 20 × 1.6	Not found	Not found	5.4	Not found
[19]	4	FR4	Metamaterial	− 17	Easy	8:9.25	120 × 90 × 1.6	Not found	Not found	7	88%
[20]	4	RO4003 $\varepsilon r = 3.55$	Decoupling lines	− 20	Medium	24:40	13.75 × 13.7 × 0.787	10	0.15	5	85%
Pro-posed design	2	FR4	Decoupling surface on ground	− 30	Easy	27:40 Especially 28 and 38 GHz	55.27 × 27.635 × 1.6	10	$< 1 \times 10^{-4}$	10	95%

Abbreviations

MIMO	Multiple input multiple output
DG	Diversity gain
CLL	Channel loss capacity
ECC	Envelope correlation coefficient
MEG	Mean effective gain
HPBW	Half power beam width
MLM	Mean loop magnitude
SLL	Side-lobe level

Acknowledgements
We are grateful to anyone who have contributed to the enhancement of the paper's completeness.

Author contributions
This paper is completed with the cooperation of four authors. All authors read and approved the final manuscript.

Funding
Open access funding provided by The Science, Technology & Innovation Funding Authority (STDF) in cooperation with The Egyptian Knowledge Bank (EKB).

Availability of data and materials
The experimental data used and/or analyzed during the current study are available from the corresponding author on reasonable request.

Declarations

Ethics approval and consent to participate
Not applicable.

Consent for publication
We agree to the publication of the paper.

Competing interests
The authors declare that they have no competing interests.

Received: 29 March 2023 Accepted: 20 June 2023
Published: 10 July 2023

References

1. T. Annalakshmi, S. Ramesh, M. Swetha Lakshmi, A tree-shaped wearable conductive fabric patch antenna for ISM band applications. in *Advances in Smart System Technologies*. Springer, Singapore, 293–301 (2021)
2. C. Mukta, M. Rahman, A.Z. Islam, Design of a compact circular microstrip patch antenna for WLAN applications. Int. J. Ad Hoc Netw. Syst. (IJANS) **11**(3), 1–12 (2021)
3. S.R. Best, A discussion on the significance of geometry in determining the resonant behavior of fractal and other non-euclidean wire antennas. IEEE Antennas Propag. Mag. **45**(3), 9–28 (2003). https://doi.org/10.1109/MAP.2003.1232160
4. R. Steven, Best, operating band comparison of the perturbated sierpinski and modified parany gasket antennas. IEEE Antennas Wirel. Propag. Lett. **1**, 35–38 (2002). https://doi.org/10.1109/LAWP.2002.802584
5. E. Guarigli, S. Silvestrov, Fractional-wavelet analysis of positive definite distributions and wavelets on D'(C). Engineering mathematics II: algebraic, stochastic and analysis structures for networks, data classification and optimization. Springer International Publishing, 337–353 (2017).
6. C. Puente-Baliarda, J. Romeu, R. Pous, A. Cardama, On the behavior of the Sierpinski multiband fractal antenna. IEEE Trans. Antennas Propag. **46**(4), 517–524 (1998). https://doi.org/10.1109/8.664115
7. K.C. Hwang, A modified sierpinski fractal antenna for multiband application. IEEE Antennas Wirel. Propag. Lett. **6**, 357–360 (2007). https://doi.org/10.1109/LAWP.2007.902045
8. J. Anguera, C. Borja, C. Puente, Microstrip fractal-shaped antennas: a re microstrip fractal-shaped antennas: a review. in *The second european conference on antennas and propagation,* EuCAP 2007. IET, 1–7 (2007). https://doi.org/10.1049/ic.2007.1521.
9. N. Ojaroudi Parchin, H. Jahanbakhsh Basherlou, M. Alibakhshikenari, Y. Ojaroudi Parchin, Y.I. Al-Yasir, R.A. Abd-Alhameed, E. Limiti, Mobile-phone antenna array with diamond-ring slot elements for 5G massive MIMO systems. Electronics **8**, 1–17 (2019)
10. Y. Nanae, S. Chulhun, A 28-GHz wideband 2 × 2 U-slot patch array antenna. J. Electromagn. Eng. Sci. (2017). https://doi.org/10.5515/JKIEES.2017.17.3.133
11. R. Anitha, P.V. Vinesh, K.C. Prakash, P. Mohanan, K. Vasudevan, A compact quad element slotted ground wideband antenna for MIMO applications. IEEE Trans. Antennas Propag. **64**(10), 4550–4553 (2016)
12. A.A. Althuwayb, Low-interacted multiple antenna systems based on metasurface-inspired isolation approach for MIMO applications. Arab. J. Sci. Eng. (2021). https://doi.org/10.1007/s13369-021-05720-6
13. H.X. Xu, G.M. Wang, J.G. Liang, M.Q. Qi, X. Gao, Compact circularly polarized antennas combining meta-surfaces and strong space-filling meta-resonators. IEEE Trans. Antennas Propag. **61**(7), 3442–3450 (2013)

14. M. Khalid et al., 4-Port MIMO antenna with defected ground structure for 5G millimeter wave applications. Electronics **9**(1), 1–13 (2020). https://doi.org/10.3390/electronics9010071
15. F. W. Ardianto, F. F. Lanang, S. Renaldy, T. Yunita, U-slot rectangular patch array for 5G Applications. In: *International Symposium on Antennas and Propagation (ISAP)*. IEEE, 23–26 (2018).
16. Y. Rahayu, I. R. Mustofa, Design of 2 × 2 MIMO Microstrip Antenna Rectangular Patch Array for 5G Wireless Communication Network. in *Progress in Electromagnetics Research Symposium—Fall (PIERS—FALL)*. IEEE, 2679–2683 (2017). https://doi.org/10.1109/PIERS-FALL.2017.8293591.
17. M. K. Ishfaq, T. Abd Rahman, Y. Yamada, K. Sakakibara, 8×8 Phased series fed patch antenna array at 28 GHz for 5G mobile base station antennas. in *International Conference on Info com Technologies and Unmanned Systems (Trends and Future Directions) (ICTUS)*, 160–162 (2017). https://doi.org/10.1109/APWC.2017.8062268.
18. Y. Wang, D. Piao, A compact size dual-polarized high-gain resonant cavity antenna at 28 GHz. in *International Applied Computational Electromagnetics Society Symposium (ACES)*. IEEE, 1–2 (2017).
19. A. Thatere, P. L. Zade, D. Arya, Bandwidth enhancement of microstrip patch antenna using 'U' slot with modified ground plane. in *2015 International Conference on Microwave, Optical and Communication Engineering (ICMOCE)*, 408–411 (2015). https://doi.org/10.1109/ICMOCE.2015.7489779.
20. I. Rosaline, A. Kumar, P. Upadhyay, A.H. Murshed, Four element MIMO Antenna systems with decoupling lines for high-speed 5G wireless data communication. Int. J. Antennas Propag. (2022). https://doi.org/10.1155/2022/9078929
21. K.S. Sultan, H.H. Abdullah, Planar UWB MIMO-diversity antenna with dual notch characteristics. Progres. Electromagn. Res. C. **93**, 119–129 (2019). https://doi.org/10.2528/PIERC19031202
22. R.E. Shehata, A. Elboushi, M. Hindy, H. Elmekati, Metamaterial inspired LPDA MIMO array for upper band 5G applications. Int. J. RF Microw. Comput. Aided Eng. **32**(8), 1–14 (2022). https://doi.org/10.1002/mmce.23212
23. D.A. Sehrai, M. Abdullah, A. Altaf et al., A novel high gain wideband MIMO antenna for 5G millimeter wave applications. Electronics **9**(6), 1031 (2020). https://doi.org/10.3390/electronics9061031
24. J.A. Sapna Verma, Ansari, analysis of U-slot loaded truncated corner rectangular microstrip patch antenna for broadband operation. AEU-Int. J. Electron. Commun. **69**(10), 1483–1488 (2015). https://doi.org/10.1016/j.aeue.2015.07.002

Publisher's Note